**Title:** Inflammasome mediated neuronal-microglial crosstalk: a therapeutic substrate in *C9orf72*-FTD/ALS.

**Authors**: Kyle J. Trageser[1‡], Chad Smith[1‡], Maria Sebastian-Valverde[1], Umar Haris Iqbal[1], Henry Wu[1], Molly Estill[2], Md Al Rahim[1], Urdhva Raval[1], Francis J Herman[1], Emma Zeng[1], Ruth Iban Arias[1], Tatsunori Oguchi[1], Yon-Jie Zhang[3], Leonard Petrucelli[3], Giulio Maria Pasinetti[1,4]

**Affiliations:**

[1]Department of Neurology, Icahn School of Medicine at Mount Sinai, New York, New York 10029

[2]Department of Neuroscience, Icahn School of Medicine at Mount Sinai, New York, New York 10029

[3]Department of Neuroscience, Mayo Clinic, Jacksonville, FL 32224

[4]Geriatric Research, Education and Clinical Center, James J. Peters Veterans Affairs Medical Center, Bronx, New York 10468

[‡] Co-first authors

**Running title:** Inflammasome mediated pathogenesis of C9orf72-FTD/ALS

Key words: amyotrophic lateral sclerosis, frontotemporal dementia, microglia, C9orf72, neuroinflammation, neurodegeneration, inflammasome

*To whom correspondence should be addressed:
Giulio Maria Pasinetti, M.D., Ph.D.
Department of Neurology
The Mount Sinai School of Medicine
1 Gustave L. Levy Place, Box 1137
New York, NY 10029
Phone: (212) 241-7938
Fax: (212) 876-9042
Email: giulio.pasinetti@mssm.edu

## Introductory Paragraph

Intronic $G_4C_2$ hexanucleotide repeat expansions of *C9orf72* are the most common cause of familial variants of frontotemporal dementia / amyotrophic lateral sclerosis (FTD/ALS)[1,2]. $G_4C_2$ hexanucleotide repeat expansions (HREs) in *C9orf72* undergo non-canonical repeat associated translation, producing dipeptide repeat (DPR) proteins, with various deleterious impacts on cellular homeostasis[3]. While five different DPRs are produced, poly(glycine-arginine) (GR) is amongst the most toxic, and is the only DPR to accumulate in the associated clinically relevant anatomical locations of the brain[4,5]. Previous work has demonstrated the profound effects of a poly(GR) model of c9FTD/ALS, including motor impairment, memory deficits, neurodegeneration, and neuroinflammation[6]. Neuroinflammation is hypothesized to be a driving factor in the disease course; microglia activation is present prior to symptom onset and persists throughout the disease[7]. Here, we establish the contributions of the NLRP3 inflammasome in the pathogenesis of FTD/ALS, resulting from a stress-induced neuronal-microglial crosstalk feedforward loop. In a mouse model of c9FTD/ALS, inflammasome-mediated inflammation was increased with microglial activation, cleavage of caspase-1, upregulation of *Cxcl10*, and production of IL-1β. We find that genetic ablation of *Nlrp3* protected behavioral deficits and prevented neurodegeneration as seen in C57BL6J Wild Type mouse model of c9FTD/ALS. Ultimately, survival was improved by the genetic ablation of *Nlrp3*. Moreover, we identified the process by which neuronal stress signals induced by hexanucleotide expansions initiate an inflammatory cascade in microglia. These findings provide evidence of the integral role of inflammasome-mediated innate immunity in c9FTD/ALS pathogenesis, and suggest the NLRP3 inflammasome as a therapeutic target.

**Main Text**

To directly investigate the effects of GR induced neuronal stress in the brain in c9FTD/ALS, neonatal intracerebroventricular injections of adeno-associated virus serotype 9 ($AAV_9$) vectors containing either GFP (control) or 100 repeats of the GR dipeptide (GFP-$(GR)_{100}$), was conducted, as previously reported[6]. $AAV_9$ have a strong expression pattern in neurons of the brain, but not microglia[8], allowing for the targeted investigation of neuronal induced effects. Body weight of GFP and GFP-$(GR)_{100}$ mice did not differ throughout the study (**Supplementary Figure 1a**).

Examination of c9FTD/ALS behavioral features in GFP-$(GR)_{100}$ revealed significant mortality over the course of the paradigm, with over 25% of animals dying before completion (**Fig 1a**). To assess behavioral responses, mice were tested for contextual and cued memory, motor function, and anxiety. GFP-$(GR)_{100}$ animals exhibited a significant reduction in freezing in both the contextual and cued memory paradigms (**Figs 1b-c**). GFP-$(GR)_{100}$ animals exhibited a significant increase in falls in the hanging wire test (**Fig 1d**). GFP-$(GR)_{100}$ mice exhibited anxiety with an increase in thigmotaxis in the Open Field Test (**Fig 1e**). The observed impairments in motor function, memory, anxiety, as well as mortality largely replicate those seen in c9FTD/ALS.

Next, as we hypothesized the inflammasome contributes to the neurodegeneration in behaviorally relevant brain regions in the central nervous system in c9FTD/ALS, we quantified GFP-expressing neurons, indicating virally infected cells, in brain regions with major contributions to the observed behavioral phenotype. These include the prefrontal cortex (PFC), the parietotemporal lobes of the cortex (CTX), and the hippocampus (HP). This GFP-$(GR)_{100}$ model of c9FTD/ALS has previously been shown to not effect spinal cord pathology, allowing for

specific evaluation of associated brain pathologies[6]. GFP-$(GR)_{100}$ mice exhibit significant reduction in GFP-expressing neurons in the CTX, PFC, and HP (**Fig 1g-i**). Representative images are depicted in **Figure 1f.**

Microglia mediated neuroinflammation has been described in cases of ALS[9]. Microgliosis has also been previously described to occur in this model, beginning at 1.5 months of age[6]. We hypothesized that microglia, the innate immune cells of the brain, may be causally related to the pathogenesis of c9FTD/ALS. To determine microglial response to the disease process, we first stereologically quantified the density of microglia in the cortex, a relevant region of the brain that contributes to the behavioral impairments we observed in GFP-$(GR)_{100}$ and found a significant increase in GFP-$(GR)_{100}$, compared to GFP controls (**Fig 1k**). We next performed quantitative morphological analyses to characterize activation states microglia. In CTX of GFP-$(GR)_{100}$ mice, there was a trending increase in the level of ramifications closer to the soma, indicated by the increase in intersecting segments within 10 µm of the soma (**Fig 1i**) suggesting microglia hyperramification, compared to GFP controls. This is accompanied by a statistically significant decrease in the number of intersecting segments further away from the soma (20 – 30 µm away from the soma) (**Fig 1i**), indicative of an activated state described by microglia branch contraction accompanied with increased branch complexity, as depicted by a representative microglia *in situ* in (**Figure 1j.II)**. This increased density and morphological ramification of microglia in the CTX is indicative of a neuroinflammatory response occurring in GFP-$(GR)_{100}$ mice.

Next, we investigated the effects of microglial activation seen in GFP-$(GR)_{100}$ animals. We hypothesized that NLRP3 inflammasome responses may be related to the neuronal stress induced by GFP-$(GR)_{100}$. NLRP3 inflammasome complexes contain pro-caspase-1, which is

cleaved to active-caspase-1, which in turns processes the zymogenic forms of IL-1β and IL-18 into active forms; as such, we measured levels of pro-caspase-1 and active-caspase-1 via Western Blot in the cortex, and IL-1β and IL-18 via ELISA. GFP-$(GR)_{100}$ mice exhibit an increase in active caspase 1 (**Fig 1m**), pro-caspase-1 (**Fig 1n**) and the ratio of active caspase-1 to pro-caspase-1 (**Fig 1o**), in the CTX. Additionally, IL-1β was significantly increased in the CTX of GFP-$(GR)_{100}$, compared to GFP controls, while there was no change in IL-18 (**Fig 1q-r**). Collectively, the elevation of active caspase-1, pro-caspase-1, IL-1β, microgliosis and activation of microglia suggests that there is a significant innate immune driven response *in vivo* in GFP-$(GR)_{100}$ mice as a result of inflammasome assembly and activation in microglia.

Based upon our results identifying significant innate immune related inflammation in a GFP-$(GR)_{100}$ model of c9FTD/ALS, we targeted the NLRP3 inflammasome complex via genetic ablation. To test the effects of genetic ablation of *Nlrp3*, GFP-$(GR)_{100}$ or GFP expression in the mouse brain was achieved by neonatal intracerebroventricular injections of adeno-associated virus serotype 9 (AAV9) vectors in mice lacking the *Nlrp3* gene ($Nlrp3^{-/-}$). Weights of $Nlrp3^{-/-}$-GFP and $Nlrp3^{-/-}$-GFP-$(GR)_{100}$ did not differ over the course of the study (**Supplementary Figure 1b**).

Examination of the behavioral effects of inflammasome targeted interventions revealed no change in mortality in $Nlrp3^{-/-}$ GFP-$(GR)_{100}$ compared to $Nlrp3^{-/-}$ GFP and WT-GFP over the course of the experimental paradigm (**Fig 2a**). Assessment of memory function demonstrated unaffected contextual memory in $Nlrp3^{-/-}$-GFP-$(GR)_{100}$ animals compared to $Nlrp3^{-/-}$-GFP; however, significant cued memory deficits are still evident (**Fig 2b-c**). Motor function, which was significantly impaired in WT-GFP-$(GR)_{100}$, remained unaffected in $Nlrp3^{-/-}$ GFP-$(GR)_{100}$, with animals performing at a statistically similar level to $Nlrp3^{-/-}$-GFP and WT-GFP animals. (**Fig 2d**). Anxiety, as assessed by the OFT, revealed no changes in $Nlrp3^{-/-}$-GFP-$(GR)_{100}$ animals

compared to *Nlrp3*$^{-/-}$-GFP (**Fig 2e**). Interestingly, both *Nlrp3*$^{-/-}$-GFP and *Nlrp3*$^{-/-}$ GFP-$(GR)_{100}$ exhibited less freezing time in both the contextual memory task, while exhibiting a greater preference for the center zone than WT-GFP.

We next investigated the effects of targeting the NLRP3 inflammasome on neurodegeneration. GFP-$(GR)_{100}$ mice. In the CTX, no change in the count of GFP-expressing neurons was noted in *Nlrp3*$^{-/-}$-GFP-$(GR)_{100}$ compared to either WT-GFP or *Nlrp3*$^{-/-}$-GFP (**Fig 2g**). Lack of neurodegeneration in the CTX and protection in the associated behavioral tasks indicate a role of *Nlrp3* in c9FTD/ALS pathogenesis.

As we above demonstrated the presence of inflammasome mediated neuroinflammation in the cortex in GFP-$(GR)_{100}$ mice, we further investigated these findings in the cortex of *Nlrp3*$^{-/-}$-GFP-$(GR)_{100}$ mice. To assess levels of proinflammatory cytokines produced as a result of activation of inflammasome activation in response to GFP-$(GR)_{100}$, we quantified levels of IL-1β and IL-18 in the CTX of WT-GFP, *Nlrp3*$^{-/-}$-GFP, and *Nlrp3*$^{-/-}$-GFP-$(GR)_{100}$ mice. *Nlrp3*$^{-/-}$-GFP-$(GR)_{100}$ mice exhibited a significant increase in IL-1β, compared to WT-GFP controls (**Fig 2h**). Interestingly, IL-18 production was significantly lower in both *Nlrp3*$^{-/-}$-GFP and *Nlrp3*$^{-/-}$-GFP-$(GR)_{100}$ compared to WT-GFP mice (**Fig 2i**). We next assessed the levels of the pro-IL-1β and pro-IL-18 processing caspase-1. No change in active caspase-1 (**Fig 2j**), pro-caspase-1 (**Fig 2k**), and the ratio of active caspase-1 to pro-caspase-1 (**Fig 2l**) was seen in Nlrp3$^{-/-}$-GFP-$(GR)_{100}$ animals compared to *Nlrp3*$^{-/-}$-GFP or WT-GFP.

Genetic ablation of the NLRP3 inflammasome prevented the significant mortality, motor impairment, contextual memory deficits, and anxiety exhibited in our WT GFP-$(GR)_{100}$ mice. Furthermore, significant protection to GFP-expressing neurons in CTX as well as the ratio of active-caspase-1 to pro-caspase-1 is conferred by *Nlrp3* ablation. Thus, these data further

support the idea of microglia driven innate immune responses in the brain to the pathogenesis of c9FTD/ALS, and identify a novel treatment strategy of targeting microglia mediated innate immune responses.

The above data demonstrate the link of innate immune driven inflammation to disease pathogenesis in GFP-$(GR)_{100}$ animals. We next investigated the transcriptional regulation of genes in the cortex, prefrontal cortex, and hippocampus of GFP-$(GR)_{100}$ mice. Principal component analysis indicated samples tend to cluster amongst treatment groups, with both cortex and pre-frontal cortex tissues clustering within treatment groups, showing similar transcriptional profiles within GFP and GFP-$(GR)_{100}$ groups (**Fig 3a**).

Using DESeq2, a total of 165 genes are differentially regulated in the cortex of GFP-$(GR)_{100}$ animals ($p_{adj} < 0.1$). Overall transcriptional patterns depicting the significantly differentially expressed genes are visualized in **Figure 3b**, with the top three mapped upregulated and downregulated genes labelled (as identified by the magnitude of $Log_2$Fold Change) (**Figure 3b**). The top upregulated mapped gene in GFP-$(GR)_{100}$ is *Cxcl10*, which has been previously shown to result in the proliferation and activation of microglia[10].

Based on our above-described *in vivo* data characterizing a causal link between inflammasome activation and neurodegeneration resulting in behavioral impairments, we hypothesized that GFP-$(GR)_{100}$ expression would invoke transcriptional changes in innate immune responses. Examination of the pathways and regulators enriched in the differentially-expressed genes using Ingenuity Pathway Analysis confirms enrichment in neuroinflammatory signaling pathways including “Complement System”, “TREM1 Signaling”, “Chemokine Signaling”, and “NF-κB Signaling”, in the cortex (**Fig 3c**). These pathways are core regulators of inflammatory

responses and microglial activation. Amongst validated genes (**Supplemental Figure 2**), we found that *Cxcl10* is significantly upregulated, with a 7-fold increase in GFP-$(GR)_{100}$ animals, compared to GFP controls (**Fig 3d**).

The transcriptomic changes exhibited in GFP-$(GR)_{100}$ animals heavily point to significant innate immune, microglia mediated responses. Our findings of significant *Cxcl10* upregulation suggests there is a neuronal signal released which can activate microglia, and induce innate immune cascades in GFP-$(GR)_{100}$ mice.

As *Cxcl10* is an important signal for the immune responses of microglia[10], we investigated the production and effects of *Cxcl10* in primary neuronal and microglial cultures, *in vitro*. We studied, *in vitro*, the neuronal effect of GFP-$(GR)_{100}$ infection on CXCL10 production, and whether CXCL10 induces microglia activation. First, we investigated whether the expression of GFP-$(GR)_{100}$ induced neuronal death *in vitro*. GFP-$(GR)_{100}$ neurons exhibited a significant increase in the release of LDH compared to GFP neurons (**Fig 4a**), confirming the GFP-$(GR)_{100}$-induced neuronal injury and death observed *in vivo*. As *Cxcl10* was shown to be highly upregulated *in vivo* in GFP-$(GR)_{100}$ mice, we hypothesized that neurons are able to produce and secrete CXCL10, in response to GFP-$(GR)_{100}$. To test this, primary cortical neurons were transfected with either $AAV_9$-GFP or $AAV_9$-$GR_{100}$ and cell supernatants were analyzed for CXCL10 concentration. GFP-$(GR)_{100}$ neurons demonstrated significantly increased production of CXCL10 compared to GFP neurons (**Fig 4b**).

As we identified *Cxcl10* is highly upregulated *in vivo*, and was determined experimentally to be significantly released by primary cortical GFP-$(GR)_{100}$ neurons *in vitro* (**Fig 4b**), we next investigated whether CXCL10 activates microglia. Tumor necrosis factor-alpha (TNF-α) constitutes a hallmark for microglia activation and has previously been shown to play an

important role in the transcriptional regulation of components of the NLRP3 inflammasome[11]. To test the ability of CXCL10 to induce TNF-α expression, primary cortical microglia cultures were treated with escalating doses of CXCL10 and the TNF-α released to cell supernatant was measured. CXCL10 significantly increased the microglial production of TNF-α in a dose-dependent manner (**Fig 4c**), while the co-treatment with a CXCL10 neutralizing antibody results in a significant reduction in the TNF-α secreted by microglia (**Fig 4d**). Finally, to analyze if CXCL10 mediates the activation of IL-1β processing inflammasome complexes, we measured the release of IL-1β from primary cortical microglia in response to escalating doses of CXCL10. There is a significant, dose-dependent escalation in the secretion of IL-1β (**Fig 4e**). Co-treatment with a CXCL10 neutralizing antibody results in a significant reduction in IL-1β released by microglia (**Fig 4f**). These data demonstrate a neuronal-microglial crosstalk whereby GFP-$(GR)_{100}$ induces secretion of neuronal CXCL10, activating a microglial innate immune response, resulting in inflammasome activation and subsequent neuroinflammation.

In conjunction with the rest of our data, these experiments suggest that neurons in c9FTD/ALS produce DAMPs such as CXCL10 as a result of GFP-$(GR)_{100}$, which significantly stimulates pro-inflammatory reactions from microglia, leading to inflammasome activation (**Fig 4g**). Targeting the resultant NLRP3 inflammasome dependent responses serves as a potent substrate for therapeutic intervention in c9FTD/ALS.

Our present study provides evidence linking inflammasome activation to neurodegeneration, and provides a basis for the investigation of innate immune inflammasome inhibitors as a treatment of disease in c9FTD/ALS. Here, we identify a key mechanism by which neuronal stress initiated by $G_4C_2$ HREs in c9FTD/ALS can activate microglia, producing an inflammasome-dependent innate immune response, which can be therapeutically targeted. As neuronal stress occurs throughout various forms of FTD/ALS[12–14], the self-perpetuating cycle of

neuronal stress inducing microglial inflammasome activation and resultant neuroinflammation may represent a conserved therapeutic substrate throughout the various disease subtypes of FTD/ALS. Ultimately, we demonstrate that by targeting microglial reactivity through inflammasome inhibition, FTD/ALS pathogenesis was significantly attenuated through the genetic ablation of *Nlrp3*. The results of these studies identify the contributions of inflammasome activation in microglia to the pathogenesis of c9FTD/ALS.

Microglial activation and the activation of the NLRP3 inflammasome have been demonstrated as crucial mediators in other neurodegenerative conditions including Alzheimer's disease[15], Parkinson's disease[16], and primary progressive multiple sclerosis [17]. Inflammation has also been noted pre-symptomatically in models of ALS[18,19] and incidence of ALS has been demonstrated to be higher in individuals who have been diagnosed with an autoimmune disease[20], indicating a putative role in the disease pathogenesis, and a target for therapeutic intervention. Neuroimaging studies conducted on individuals with ALS have demonstrated microglial activation throughout the brain[9,21]. Upon examination of the microglia in the cortex, we observed microgliosis consistent with previously identified findings[6]. Morphologically, microglia in GFP-$(GR)_{100}$ were in an activated state; these findings are congruent with those identified in other neurodegenerative diseases, including Alzheimer's Disease, in which morphologically activated microglia are present[22].

Inflammasome activation has been noted in other forms of ALS[23–25]. We noted an increase in active caspase-1, pro-caspase-1, as well as the ratio of active-caspase-1 to pro-caspase-1 in the cortex of GFP-$(GR)_{100}$ mice; these increases were attenuated via genetic ablation of *Nlrp3*. Interestingly, while IL-1β production was not attenuated by the genetic ablation of *Nlrp3*, *Nlrp3*$^{-/-}$ mice had a significantly lower level of IL-18 in the cortex compared to WT animals. This *Nlrp3*

independent production of IL-1β has been demonstrated previously, whereby *Nlrp3* deficient mice still produce IL-1β in response to a stimulus; however, IL-18 levels were significantly decreased[26]. Studies employing caspase-1 deficient mice and caspase-1 targeting treatments should be employed in the future to further evaluate the therapeutic value of targeting inflammasome-produced cytokines in FTD/ALS.

In addition to improvements in neurodegeneration and neuroinflammation, full genetic ablation of the *Nlrp3*$^{-/-}$ inflammasome conferred significant protection behaviorally in *Nlrp3*$^{-/-}$-GFP-$(GR)_{100}$ mice compared to *Nlrp3*$^{-/-}$-GFP controls; mortality was almost completely eliminated, contextual memory was preserved, motor function was protected, and there was no increase in anxiety. To determine if the NLRP3 inflammasome can be therapeutically targeted, further studies may employ experimental models whereby NLRP3 ablation by Cre dependent-designer receptor exclusively activated by designer drugs (DREADD) mice allow for temporal control of NLRP3 expression, thereby evaluating both its role in presymptomatic disease, and evaluating whether the NLRP3 inflammasome may serve as a therapeutic target after symptom onset.

*Cxcl10*, which we found to be highly upregulated in the cortex of GFP-$(GR)_{100}$ mice, encodes for a small cytokine belonging to the CXC chemokines family. Upon neuronal death, CXCL10 is produced and exerts a chemotactic function by attracting microglia and $CD8^+$ T cells, and can induce the activation of microglia, thereby causing the release of pro-inflammatory cytokines[27]. Chemotactic effects are demonstrated in our FTD/ALS model by the microgliosis in the cortex of GFP-$(GR)_{100}$ mice where we see a significant increase in the density of microglia. Neuronal stress has been demonstrated in other forms of ALS, including in cases of sporadic ALS[28]. Dysregulation of CXCL10 chemotaxis in peripheral blood cells from ALS patients has been directly observed, which was associated to increased inflammatory responses[29]. These facts

further support our *in vitro* findings, where we demonstrated that neuronal cultures expressing $(GR)_{100}$ dipeptides released higher concentrations of CXCL10, and the treatment of microglia cultures with increasing concentrations of CXCL10 promoted a dose-dependent increase in TNF-α and in IL-1β production, indicating microglial activation.

In summary, our studies identify a novel neuron-microglia crosstalk mechanism in c9FTD/ALS whereby neuronal stress induced secretion of CXCL10 triggers inflammasome activation in microglia, thereby creating a self-propagating cycle of neurodegeneration and neuroinflammation. Our findings show targeting the inflammasome responses represents a putative therapeutic strategy, as evidenced by the genetic ablation of *Nlrp3* and resultant protection from behavioral impairment and neuropathologies.

**Acknowledgements:**

This research was supported by a grant (AT008661) from the NIG's Office of Dietary Supplements (ODS) and the National Center for Complementary and Integrative Health, awarded to G.M.P. The study was supported by the generous support of the Altschul Foundation to G.M.P. G.M.P. holds a Senior VA Career Scientist Award.

We acknowledge that the contents of this study do not represent the views of the NCCIH, the ODS, the National Institutes of Health, the U.S. Department of Veterans Affairs, or the United States Government.

**Author Contributions:**

KJT and CS conducted *in vivo* experiments of the GFP-$(GR)_{100}$ model. Immunofluorescence staining, image acquisition, and analysis was performed by KJT, CS, UHI, UR, and TO. *In vitro* experiments were conducted by MSV, MAR, and RIA. Molecular analyses, including ELISA, Western Blots, and RT-qPCR were performed by KJT, CS, MSV, HW, MAR, and EZ. Bioninformatic analyses were conducted by HW and ME. Generation and purification of the GFP-$(GR)_{100}$ and GFP viruses were completed by YJZ and LP. KJT, CS, FJH, and GMP designed the project. KJT, CS, and GMP prepared the manuscript. All authors discussed and commented on the article.

**Declaration of Interests:**

The authors declare that they have no conflicts of interest with the contents of this article.

## Figures

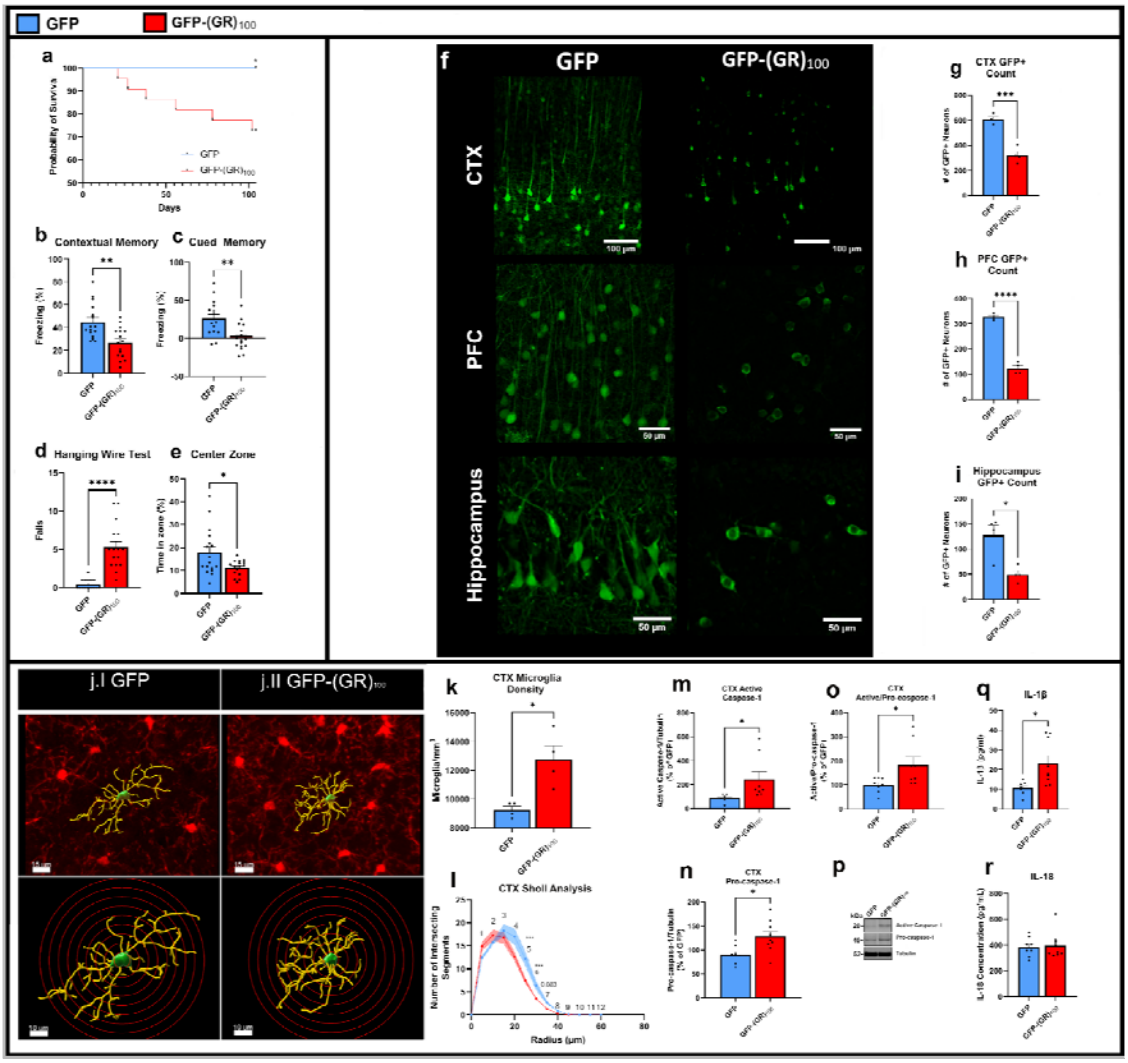


**Figure 1: Innate immune driven neuroinflammation and neurodegeneration in a GFP-$(GR)_{100}$ model of c9FTD/ALS**

Survival of GFP and GFP-$(GR)_{100}$ **(a)**. Freezing in contextual fear memory task **(b)**. Freezing in cued memory task **(c)**. Number of falls in the third day of the Hanging Wire Test **(d)**. Time spent in the central zone in the Open Field Test **(e)**. Representative GFP and GFP-$(GR)_{100}$ expressing neurons in the cortex, PFC, and hippocampal formation. Green: GFP and GFP-$(GR)_{100}$ **(f)**. Count of GFP- and GFP-$(GR)_{100}$-expression neurons in the CTX **(g)**, PFC **(h)**, hippocampus **(i)**. 3D reconstruction of microglia in the cortex, with increasing radii in 5 µm steps to measure branch intersections **(j)**. Red: Iba1 immunofluorescence. Green: Soma. Yellow: branches. Microglial density in the cortex **(k)**. Sholl analysis of microglia in cortex **(l)**. Densitometric quantification of active caspase-1 **(m)**, pro-caspase-1 **(n)**, and the ratio of active caspase-1 to procaspase-1 **(o)** in the cortex, normalized to GFP. Representative bands for caspase-1 **(p)**. 52 kDa : Tubulin. 40 kDa: Procaspase-1. 20 kDa: Active Caspase-1. Concentration of IL-1β (**q**) and IL-18 (**r**) in the CTX. Survival was analyzed by logrank test. For (b-k, m-r), * p<0.05. **p<0.01. ***p<0.001. ****p<0.0001 by Two Tailed Welch's t Test. For (l), * p<0.05. **p<0.01. ***p<0.001. ****p<0.0001 by Two Way ANOVA with Tukey's posttest. Data are presented as mean ± SEM.

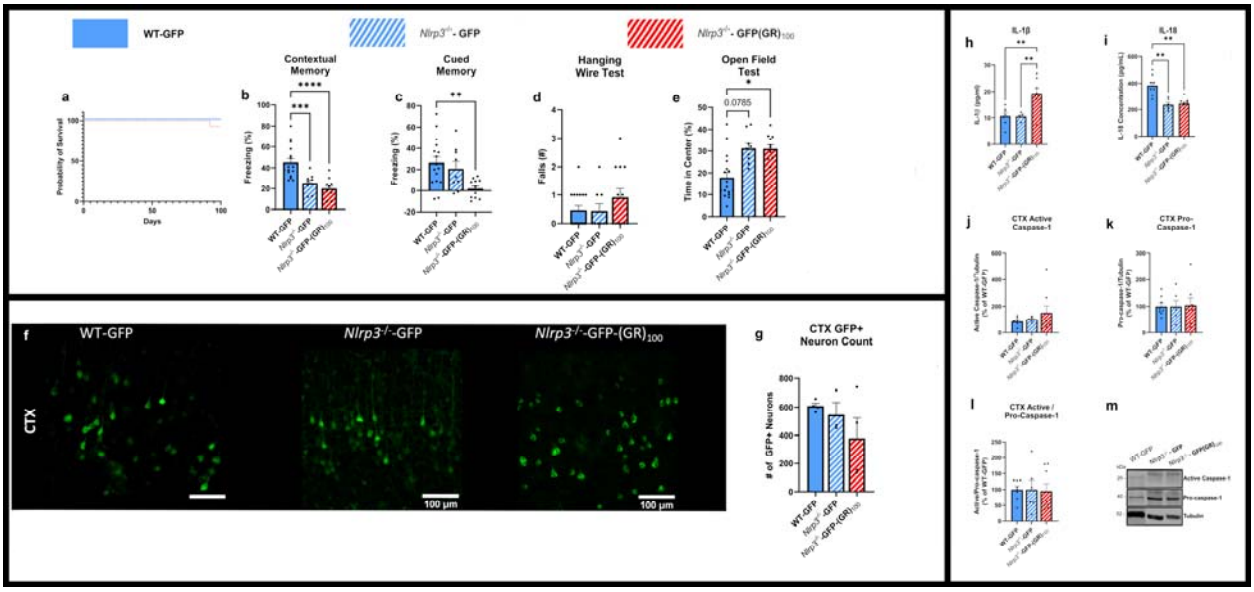


**Figure 2: Genetic ablation of NLRP3 inflammasome attenuates neurodegeneration and behavioral deficits in a GFP-$(GR)_{100}$ model of c9FTD/ALS**

Survival of WT-GFP, *Nlrp3*$^{-/-}$-GFP and *Nlrp3*$^{-/-}$-GFP$(GR)_{100}$ mice **(a)**. Freezing in contextual fear memory task **(b)**. Freezing in cued memory task **(c)**. Number of falls in the third day of the Hanging Wire Test **(d)**. Time spent in the central zone in the Open Field Test **(e)**. Representative WT-GFP, *Nlrp3*$^{-/-}$-GFP and *Nlrp3*$^{-/-}$-GFP$(GR)_{100}$ expressing neurons in the cortex, Green: GFP and GFP-$(GR)_{100}$ **(f)**. Count of GFP- and GFP-$(GR)_{100}$-expression neurons in the CTX **(g)**. Concentration of IL-1β (**h**) and IL-18 (**i**) in the CTX. Densitometric quantification of active caspase-1 **(j)**, procaspase-1 **(k)**, and the ratio of active caspase-1 to procaspase-1 **(l)** in the cortex, normalized to GFP. Representative bands for caspase-1 **(m)**. 52 kDa : Tubulin. 40 kDa: Procaspase-1. 20 kDa: Active Caspase-1.

For **(a)**, survival was analyzed by logrank test. For **(b-m)**, * p<0.05. **p<0.01. ***p<0.001. ****p<0.0001 by Two-Way ANOVA with Tukey's posttest. Data are presented as mean ± SEM. Data are presented as mean ± SEM.

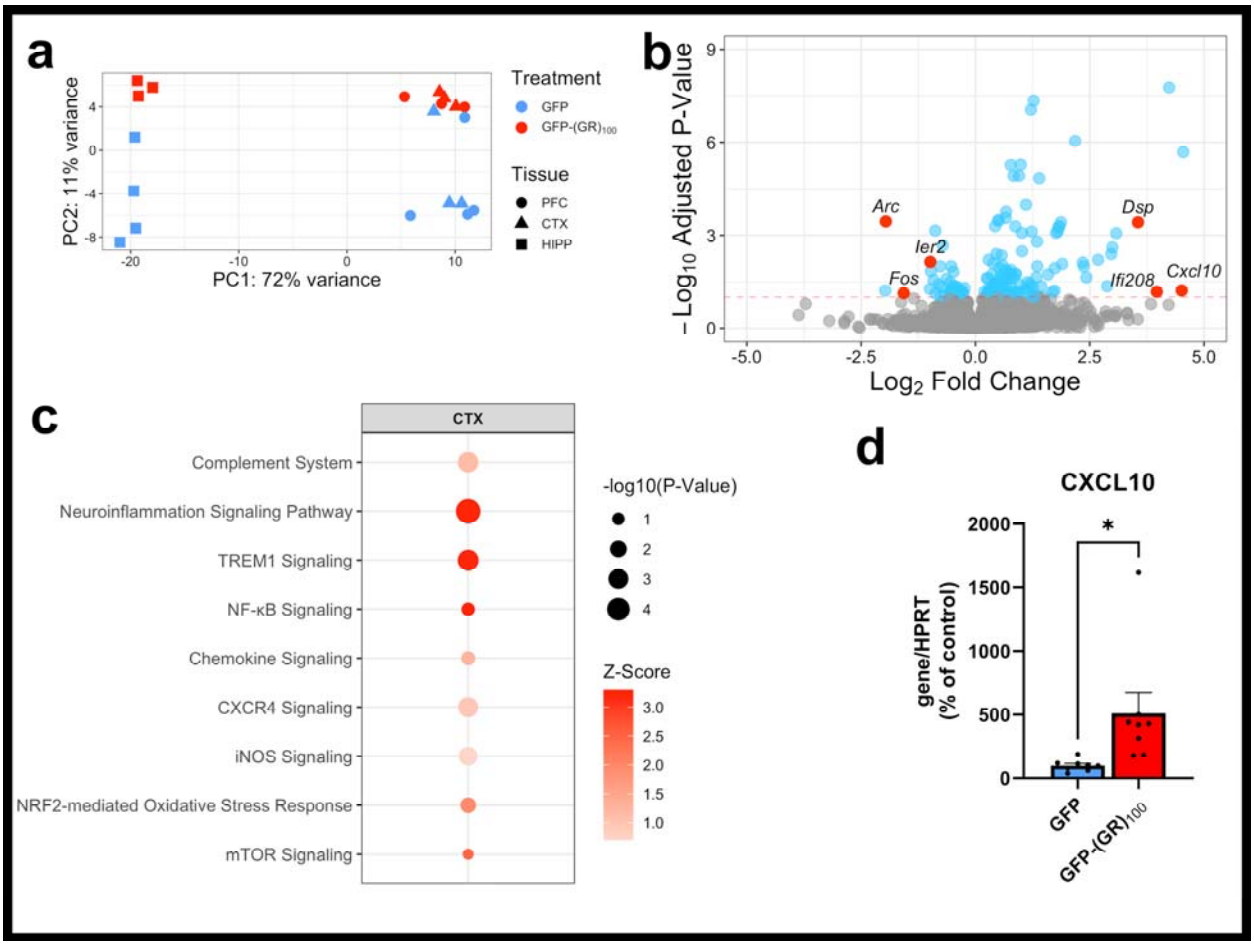


**Figure 3: Transcriptional changes of GFP-$(GR)_{100}$**

Principal component analysis (PCA) of samples. Abbreviations: Principal Component 1 (PC1); Principal Component 2 (PC2). Each point represents a single sample, with the tissue of the sample represented as a circle, triangle, or square. The treatment type is shown in red, green, or blue, for GFP and GFP-$(GR)_{100}$ **(a)**. Volcano plots of cortical gene transcription. X-axis represents the log2 fold change, while the Y-axis represents the negative log10 FDR-adjusted P-value. Genes with an adjusted P-value less than 0.10 are shown in blue. The 3 most highly upregulated mapped genes and 3 most highly downregulated genes are highlighted in red **(b)**. Inflammation related IPA pathways. Select immune system-related pathways are shown for the cortex; the p-value of each entry is represented by the size of the corresponding circle. The z-score, indicating the computed activation or repression of the given pathway, is indicated with a color gradient **(c)**. RT-qPCR validation of the most highly upregulated gene, *Cxcl10,* in the cortex of GFP and GFP-$(GR)_{100}$ mice. For d, * p<0.05 by Two tailed Welch's t Test.

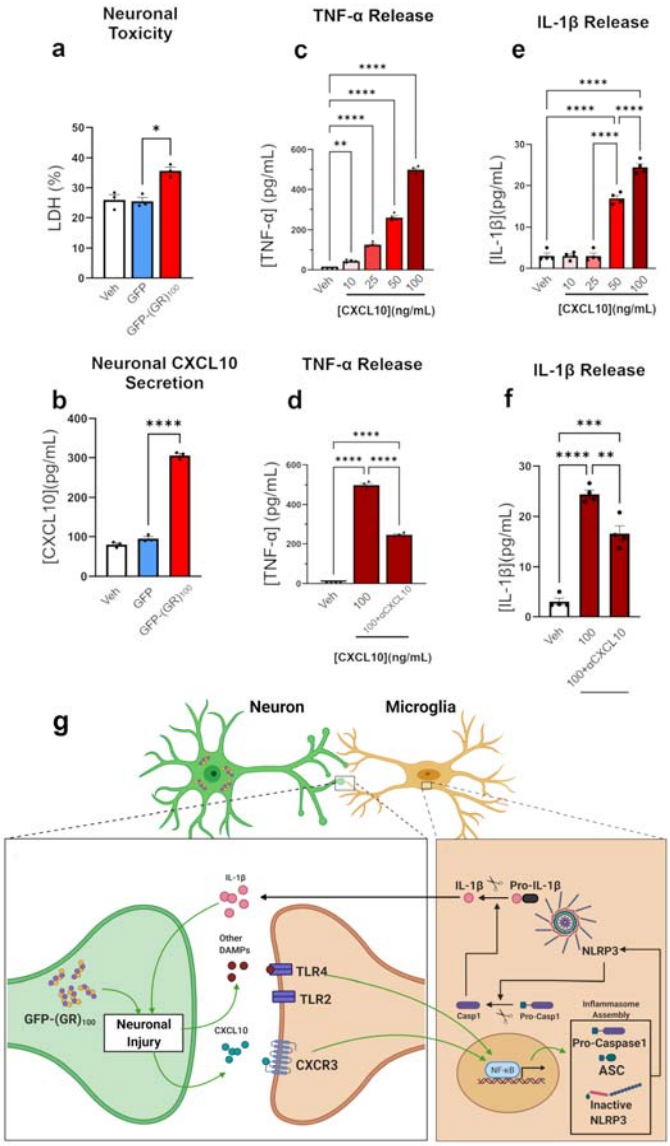


**Figure 4: *In vitro* evaluation of neuronal signaling and resultant activation microglia in c9FTD/ALS**

Evaluation of neurotoxicity of GFP-$(GR)_{100}$ **(a)**, Neuronal release of CXCL10 after infection with GFP-$(GR)_{100}$ **(b)**, CXCL10 dependent release of TNF-α **(c)**, Neutralization of CXCL10 and TNF-α release **(d)**, CXCL10 dependent release of IL-1β **(e)**, Neutralization of CXCL10 and IL-1β release **(f).** Schematized mechanism of GFP-$(GR)_{100}$ inducing neuronal release of CXCL10, which may then bind to microglial receptors and initiate an inflammasome response **(g)**. The data shown correspond to average values of biological triplicates ran in technical duplicates. For a-f, * p<0.05. **p<0.01. ***p<0.001. ****p<0.0001 by one-way ANOVA.

## Supplemental Figures

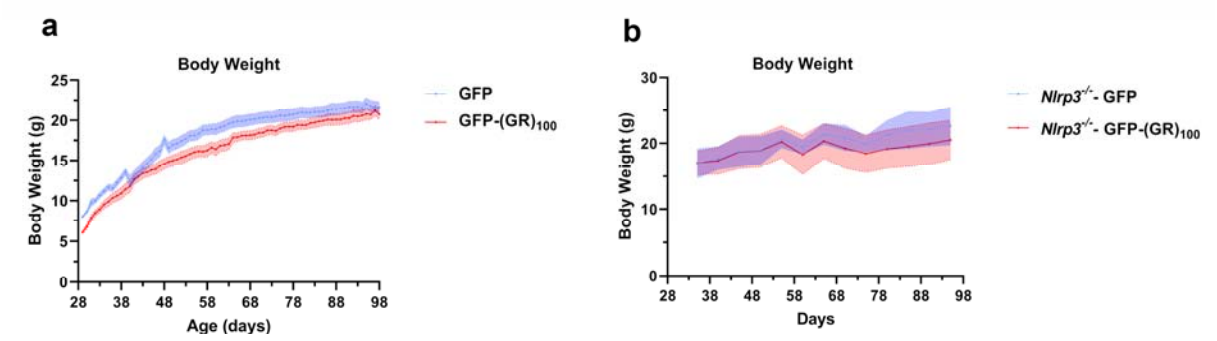


**Supplemental Figure 1**: Physiological monitoring data of GFP and GFP-$(GR)_{100}$ **(a)** and *Nlrp3*$^{-/-}$-GFP and *Nlrp3*$^{-/-}$-GFP$(GR)_{100}$ mice **(b)**

CTX

| Pathway | Gene | GFP-(GR)100 |
|---|---|---|
| Complement System | *C4b* | ** |
| | *Serping1* | ** |
| | *C4a* | ns |
| | *Itgax* | **** |
| Neuroinflammation Signaling Pathway | *Nlrc4* | * |
| | *Nlrc5* | ** |
| | *Cybb* | 0.0563 |
| | *Cxcl10* | * |
| | *Trem2* | *** |
| TREM1 Signaling | *Fcgr2b* | ns |
| | *Nlrp3* | ns |
| | *Pycard* | ns |
| | *Il1b* | ns |
| | *Il18* | ns |
| NF-κB Signaling | *Tlr4* | ns |
| | *Il1r1* | ns |
| | *Nfkbia* | ns |
| | *Tlr2* | 0.0544 |
| | *Crebbp* | ns |
| | *Ep300* | ns |
| Interferon Signaling | *Trim21* | ns |
| | *Usp18* | ** |
| | *Psmb8* | **** |
| | *Tap1* | *** |
| | *Ifit3* | ** |
| Chemokine Signaling | *Ccl2* | ** |
| | *Gnaq* | ns |
| Antigen Presentation Pathway | *H2-Q6* | 0.0617 |
| | *H2-Q7* | ns |
| Phospholipase C Signaling | *Plce1* | ** |
| | *Plcg2* | ** |
| | *Plcl2* | ns |
| | *Creb1* | ns |
| | *Map2k6* | ns |
| CXCR4 Signaling | *Cxcl12* | ns |
| iNOS Signaling | *Stat1* | 0.0603 |
| NRF2-mediated Oxidative Stress Response | *Gpx1* | ns |
| mTOR Signaling | *Rictor* | ns |
| Other | *Tnfaip1* | 0.0542 |
| | *Cd22* | ns |
| | *Slc17a6* | ns |

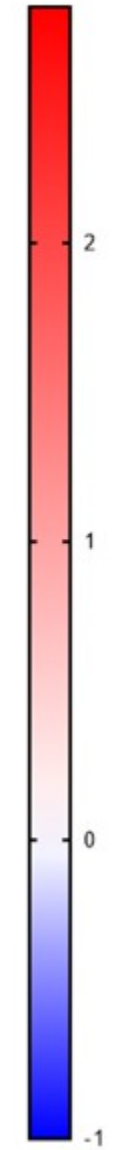


**Supplemental Figure 2**: RT-qPCR validation of significant IPA Genes identified via RNAseq. Gene ontologies are indicated on the left. Colors indicate $log_2$ fold change ($Log_2FC$). *$p$<0.05. **$p$<0.01. ***$p$<0.001. ****$p$<0.0001 by Two-Tailed Welch's t test. Statistically insignificant trends ($p$<0.1) are indicated. ns: not significant ($p$ > 0.1).

**Supplemental Table S1**
**Primers used in this study**

| | Primer, 5' -> 3' | |
|---|---|---|
| **Gene** | **Forward** | **Reverse** |
| mouse *Hprt* | CCCCAAAATGGTTAAGGTTGC | AACAAAGTCTGGCCTGTATCC |
| mouse *C4b* | GACGGGGAAACCAGTGACAA | TGAGCTCAGAGAGCCAGAGT |
| mouse *Serping1* | GAACTTGGACCAGGACGCAG | GCTGGTAGCTTCGGGATCTG |
| mouse *C4a* | ATATGCATGGAGCGCCTACG | CTTGCCATTGCGCCAGATAC |
| mouse *Itgax* | GAGGCTGCAAGCATCATTCG | GCATCAAAGTTCTCCACGCTG |
| mouse *Nlrc4* | CAGGTCACAGAAGAAGACCTGA | ACTTCCCTTTGCCAGACTCG |
| mouse *Nlrc5* | TTGCCTACTATGGGGAGCCT | AGCTCCACAAGACTCAGCAC |
| mouse *Cybb* | GAGGTTGGTTCGGTTTTGGC | GGCATCTTGGAACTCCTGCT |
| mouse *Cxcl10* | ATGACGGGCCAGTGAGAATG | GAGGCTCTCTGCTGTCCATC |
| mouse *Trem2* | ACAGCACCTCCAGGAATCAAG | AGGATCTGAAGTTGGTGCCC |
| mouse *Fcgr2b* | ATCTGGACTGGAGCCAACAAG | TTCTTCATCCAGGGCTTCGG |
| mouse *Nlrp3* | GCCATCATCAGCTCCTGTGT | ACTGGCTGACTGAACGACTG |
| mouse *Pycard* | CCGAGTTTCATCCCCAGTCC | GCCTTTGATCCCAGGCCTAT |
| mouse *Il1b* | CTCCATGAGCTTTGTACAAGG | TGCTGATGTACCAGTTGGGG |
| mouse *Il18* | AGCAGTGGTTTTCAGCTGGG | GGGAACAGCCAGTGTTCAGT |
| mouse *Tlr4* | CCTGTGGACAAGGTCAGCAA | CTCGGCACTTAGCACTGTCA |
| mouse *Il1r1* | GTCATTCTTGTGCACGCCAG | AACTGCCTCCTCAAGTCAGC |
| mouse *Nfkbia* | AGGACGAGGAGTACGAGCAA | CGTGGATGATTGCCAAGTGC |
| mouse *Tlr2* | AGGTGCGGACTGTTTCCTTC | CCGGTGATGCAATTCGGATG |
| mouse *Crebbp* | CCCACACTGTCGAACCATGA | ACAGTCATGTCGTGTGCAGT |
| mouse *Ep300* | AGGAGGAAGAACAGCCAAGC | CAGGGATTCCTAGAAGCTGCG |
| mouse *Trim21* | AGGAGAGGCTCCTGTCATTCA | GCCCCCATTCTTCCCAACTT |
| mouse *Usp18* | CAGGAGTCCCTGATTTGCGT | GGGCTGGACGAAACATCTCA |
| mouse *Psmb8* | GATGACAATGGGACTCGGCT | CTCCACTTTCACCCAACCGT |
| mouse *Tap1* | CGGCAACCTTGTCTCATTCG | CATGTTTGAGGGTGCCAACG |
| mouse *Ifit3* | GCAGCACAGAAACAGATCACC | GTTGCACACCCTGTCTTCCA |
| mouse *Ccl2* | CAGGTCCCTGTCATGCTTCT | GTGGGGCGTTAACTGCATCT |
| mouse *Gnaq* | GGTGTGCTGACCTAAGACCC | ACCCCAGGTCAAATGGCAAA |
| mouse *H2-Q6* | GTGTGACCTTGGGTCTTCATTT | TCCTGGTGTGTAGGCGAAG |
| mouse *H2-Q7* | CGGGAGCGGGTTGTAAAGT | CACCAGCAAGAGCAGCATTG |
| mouse *Plce1* | ACTCTTCTCATCCTCGGGGT | GGCTTGACTCTGGACGAACA |
| mouse *Plcg2* | GATCATGGAGACTCGGCAGG | GACAAACTGGGTGCCGTAGA |
| mouse *Plcl2* | CGCGGAGCAAAGGACAAAAA | CCGATGTAGTCGTCGTCCAG |
| mouse *Creb1* | GAGAAGCGGAGTGTTGGTGA | ACTCTGCTGGTTGTCTGCTC |
| mouse *Map2k6* | CCTGGCCCATCATGTAGCTG | CTCTTGACCGATGCAGCAGA |
| mouse *Cxcl12* | GGTGCTCAAACCTGACGGTA | CCTGGCCTTCATGGGATTGT |
| mouse *Stat1* | GTCATCCCGCAGAGAGAACG | AGGGTATGGAGCAGAGCTGA |
| mouse *Gpx1* | CAGTATGTGTGCTGCTCGGC | CATTCTCCTGGTGTCCGAACTGAT |
| mouse *Rictor* | ACTGACGCCAAGCAGGTTTA | TTCTTGCACCTCGGTCATCT |
| mouse *Tnfaip1* | GATTCGTCACTCCTGCGGAA | CTGAACGGCCAGGTTTTTGG |
| mouse *Cd22* | ACACAGGAGGAAACAGGCTT | ACCAGGAACAGGTGTAGGGA |
| mouse *Slc17a6* | TCTGTCCGTGGTCCTGAAATG | GCTGATCTTTGCGAACGTGA |

**Supplemental Table 1** : Primers used in this study

## Materials and Methods

### *Materials*

The $AAV_9$-GFP and $AAV_9$-GFP-$(GR)_{100}$ viruses were a kind gift from Dr. Leonard Petrucelli. Unless specified otherwise, cell culture reagents were obtained from ThermoFisher Scientific (Waltham, MA) and antibodies were obtained from Abcam (Cambridge, MA).

### *Subjects*

Wild-type C57BL/6J mice (#000664) and *Nlrp3*$^{-/-}$ mice (#021302) were obtained from The Jackson Laboratory (Bar Harbor, ME) and socially housed on a 12:12-h light/dark cycle with lights on at 07:00 h in a temperature-controlled (20□±□2□°C) vivarium. Mice were given food and water *ad libitum* and were bred to obtain mouse pups used in our studies. All procedures were approved by the Institutional Animal Care and Use Committee of the Icahn School of Medicine at Mount Sinai.

### *C9orf72 dipeptide model of frontotemporal dementia / amyotrophic lateral sclerosis*

Upon confirmation of pregnancy, wild-type and *Nlrp3*$^{-/-}$ dames were separated and monitored daily for litters. After identification of a milk spot to confirm that newborn (p0) pups were being nursed, the pups were injected with $AAV_9$-GFP or $AAV_9$-GFP-$(GR)_{100}$ by the ICV method. Pups were cryoanesthetized by placing in a padded 15mL tube partially submerged in a slurry of water and crushed ice. Upon confirmation of anesthesia by toe-pinch, we identified the point of injection, approximately two-fifths of the distance between bregma and each eye. A Hamilton syringe (#7634-01; Reno, NV) with a 32 ga needle (10 mm long, Hamilton #7803-04) was loaded with 4 µL of the AAV vector and placed 2 mm deep, orthogonal to the mouse's head at the point of injection. 2 µL of the AAV vector was injected at a rate of 1 µL min$^{-1}$ into each lateral ventricle. Upon completion of injections, each pup was rapidly returned to physiological

496 temperatures by placing on a warming pad. The litters were returned to dames upon completion
497 of injection for the entire litter and monitored for acceptance. Mice were weaned at p30 by sex.
498 For confirmation of diffusion prior to studies, a small number of mice were injected with Trypan
499 Blue and sacrificed two hours later for dissection of the brain and examination by stereoscopic
500 microscope.

501 *Behavioral testing*

502 After reaching 3 months of age, mice were tested through a battery of behavioral tests. All
503 behavioral testing took place during the light phase of the day (9:00AM). On all days of
504 behavioral testing, mice were acclimated to an anteroom directly adjacent to the behavioral
505 testing room for 30 min. On Day One, mice were tested in the Open Field Test for basal anxiety
506 and general locomotor impairments (Seibenhener et al., 2015). The Open Field apparatus
507 consisted of a 40cm x 40cm x 40cm Plexiglass box with opaque white walls, situated within a
508 dimly-lit room (200 lux). Mice were placed in the center of the apparatus and were allowed to
509 freely explore for 10 minutes before being returned to their home cage. On Day Three through
510 Five, mice were tested in a Hanging Wire Test for muscular impairments (Aartsma-Rus and van
511 Putten, 2014). The Hanging Wire apparatus consisted of a 2mm-thick wire suspended 35cm
512 over a layer of corn cob bedding, situated in a brightly lit room (500 lux). Mice were lifted from
513 their home cage by the base of their tail and were placed near the wire until they grasped it with
514 their forelimbs. The number of falls over a 2 min period were recorded. Falls in which the mice
515 hanged from the wire from their hindlimbs were excluded from the number of falls. At the end of
516 the behavioral trial, mice were returned to their home cages. On Days Seven through Nine,
517 mice were tested in a Contextual and Cued Memory Test in two Contexts. Context A was a
518 30cm x 24cm x 21cm conditioning chamber (Med Associates, Fairfax VT) within a room with
519 white walls and bright lighting. Context A had a bare metal grid floor, bare grey walls, bright
520 lighting, and background fan noise. Context A was cleaned with a 0.5% hydrogen peroxide

solution (Virox, Oakville Canada) between each trial. Context B was a chamber of the same dimensions within a room with dim lighting. The chamber had a white plastic floor, curved white plastic walls, dim lighting, no background fan noise, and scented with 0.25% benzaldehyde in 70% ethanol. Context B was cleaned with a 70% ethanol solution between each trial. On Day Seven, mice were allowed to explore Context A for 4 min. At 180s, white-noise (85 dB) played for 30 s and was co-terminated with a footshock (2 s, 0.75 mA). After the 4 min trial, the mouse was returned to its home cage. On Day Eight, mice were allowed to explore Context A for 4 min in the absence of white-noise and footshock (Context Recall). On Day Nine, mice were allowed to explore Context B in the constant presence of white-noise (85 dB, Cue Recall). For all tasks, behavior was analyzed and recorded with Any-Maze v6.0 (Stoelting, Wood Dale IL).

*Immunofluorescence*

After completion of behavioral studies, a subset of mice were deeply anesthetized with ketamine/xylazine (100 mg/kg + 10 mg/kg, IP), then were perfused transcardially with cold sterile PBS followed by 4% PFA in PBS. Brains were removed, drop-fixed in 4% PFA overnight, then washed once with cold PBS and stored in PBS. Tissue sections (50 µm thick) were taken with a vibratome (Leica; Wetzlar, Germany) and were stored in PBS with 0.02% sodium azide (w/v). Sections were washed in PBS followed by 10 min permeabilization in 0.1% Triton X-100 in PBS (PBST). Sections were then incubated in blocking solution (5% goat serum in PBST) for 1.5 hr. The sections were washed three times with PBST and incubated with primary antibodies diluted in blocking solution: 1:500 Rabbit anti-Iba1 (ab178846, Abcam) and 1:250 chicken anti-GFP (A10262, ThermoFisher) overnight at 4°C. Post incubation, the sections were washed three times in PBST and incubated with secondary antibodies diluted in blocking solution for two hours at room temperature: Goat anti-Rabbit conj AlexaFluor 568 (Abcam #175471, 1:500) and 1:500 Goat anti-Chicken AlexaFluor 488 (A11039, Thermofisher). The sections were washed three times in PBST and incubated in 1µM DAPI solution (ab228549, Abcam) for 5 min. The

546 sections were washed twice in PBS and mounted on slides using ProLong Diamond Antifade
547 Mountant (P36970, ThermoFisher).

548

549 *Stereology and cell morphology*

550 Sections were stained for immunofluorescence as described above. Microglia density for the
551 cortex, prefrontal cortex, and hippocampus of the brain was determined through the use of MBF
552 Stereo Investigator (Williston VT). The number of sections required for each region were
553 determined by an initial pilot study which found that six sections were needed for both cortex
554 and prefrontal cortex regions and seven sections for the hippocampal region, each spaced
555 equidistantly. A widefield microscope (AxioImager M2/Z2, Carl Zeiss, Oberkochen Germany)
556 along with MBF Stereo Investigator were used to visualize each section and to determine the
557 number of microglia in each region. Using the Optical Fractionator workflow, the region of
558 interest was traced onto each section based on the mouse brain atlas by Paxinos and Franklin
559 (Paxinos and Franklin). This was followed by a systematically random grid overlay consisting of
560 squares measuring 300 µm by 300 µm, covering the region of interest. From each of these
561 squares an unbiased sampling region (100 µm by 100 µm) was used to manually count
562 microglia somata in the area. Once each section was completed, the software ran an algorithm
563 to estimate the number of microglia in the region. In parallel, the Cavalieri estimator in the
564 software was used to determine the volume of each region. The microglia count and volume
565 were then used to determine the microglia density in the CTX, PFC, and hippocampal regions.
566 For assessment of cell morphology, images of coronal sections were taken on a Zeiss LSM880
567 Airyscan confocal microscope (Oberkochen, Germany) using an X20/0.8 NA air immersion
568 objective controlled by Zeiss Zen Black software. For 3D analysis, z-stack images were
569 obtained by capturing an image every 0.7µm covering the entire 50µm-thick section. Images

were deconvoluted using AutoQuant X3.1 (Media Cybernetics, Rockville MD) and 3D analysis was performed using Imaris 9.1.2 (Bit Plane Inc, Concord MA) using the surface tool to reconstruct the soma and the filaments tool to reconstruct the branches.

*Microglial cultures*

Cortices from 1-3 day-old C57BL/6J mouse pups were isolated, digested, and seeded at a density of 8 cortices per 10 mL culture dish. Every three days, medium (DMEM + 10% FBS + 1% penicillin-streptomycin) was replenished. After 3 weeks, mixed glial cultures reached confluence and were isolated by mild trypsinization as previously described (Saura et al., 2003). Briefly, cells were washed with culture medium without FBS and treated with a mixture of trypsin (0.25% without EDTA) and DMEM-F12 medium in a 1:3 ratio. After 40 min incubation, mixed glial cells detached and left a layer of microglia attached to the bottom of the culture dish. Pure microglia were isolated by 15 min incubation with trypsin (0.05% with EDTA) at 37°C followed by gentle shaking. Cells were counted and seeded in 24-well plates at a density of $7.5 \times 10^4$ cells/wells.

*Cortical neuron cultures*

Cortices from 3-day old C57BL/6J mouse pups were isolated and finely diced in ice-cold HBSS. Cortices were then incubated in 10X Trypsin Solution (Sigma #59427C) with DNase I (Sigma #D4513) for 15 min at 37°C with period inversion. Cells were then spun at 200g for 5 min, and the pellet was triturated with a serological pipette and strained in a 40 µm cell strainer (BD Falcon #352340). Centrifugation followed by trituration was repeated once, then the pellet was spun down and resuspended in Neurobasal medium supplemented with 0.25% GlutaMAX, 2% B-27, 10% Fetal Bovine Serum, and 1% Penicillin/Streptomycin at a density of $5 \times 10^5$ cell/mL. 2 hours later, medium was changed to Neurobasal medium supplemented with 0.25% GlutaMax, 2% B-27, and 1% Penicillin/Streptomycin, and half the medium was replenished every 3-4 days

afterwards. 3 days later, cells were infected with 2 x $10^{10}$ vg/mL AAV. Expression was confirmed by fluorescence microscopy. Cell supernatant and lysates were collected for assessment of LDH release and CXCL10 production (R&D Systems #DY466).

*Analysis of Cytokines and Caspase-1 activity*

After completion of behavioral trials, a subset of mice were sacrificed and brain regions were immediately frozen on dry ice and plasma was isolated from trunk blood using Lithium Heparin-treated tubes (Becton Dickinson #365985, Franklin Lakes NJ). Brain regions were lysed with 1X Cell Lysis Buffer supplemented with 1 mM PMSF (Cell Signaling #8553S, Danvers MA) and Protease Inhibitor Cocktail (Sigma-Aldrich, #11873580001). IL-1β in brain tissue, plasma, and microglia culture supernatant was measured with Mouse IL-1 beta/IL-1F2 DuoSet ELISA Kit (R&D Systems DY401, Minneapolis MN) according to the manufacturer's instructions. CXCL10 was measured in neuronal culture supernatant with Mouse CXCL10 DuoSet ELISA (R&D Systems DY466-05, Minneapolis MN) according to manufacturer's instructions. Primary microglia were stimulated with recombinant Mouse CXCL10 protein (R&D Systems 466-CR-050/CF, Minneapolis MN) and incubated with Mouse CXCL10 antibody (R&D Systems AF-466-NA, Minneapolis MN). TNF-α and IL-1β were measured in supernatant by ELISA with Mouse TNF-alpha Quantikine ELISA Kit (R&D Systems MTA00B, Minneapolis MN) and Mouse IL-1 beta/IL-1F2 DuoSet ELISA Kit (R&D Systems DY401, Minneapolis MN) according to manufacturer's instructions. For analysis of caspase-1 activity, 35 µg of protein was loaded into a Western blot using a PVDF membrane (Bio-Rad #1620177; Hercules, CA) with Mouse IL-1 beta/IL-1F2 DuoSet ELISA Kit (R&D Systems DY401, Minneapolis MN) according to the manufacturer's instructions. Membranes were blocked with 5% Bovine Serum Albumin (BSA) in 0.1% TBST and were probed with the following antibodies. Primary antibodies: Mouse anti-Caspase-1 1:1000 (AdipoGen #AG-20B-0042; San Diego, CA), Mouse anti-Tubulin 1:1000

(Sigma #T9026). Secondary antibodies: Goat anti Mouse conj HRP (1:10000, ThermoFisher #G-21040).

*Gene expression and RNAseq*

After completion of behavioral trials, a subset of mice were sacrificed and brain regions were immediately frozen on dry ice. Total RNA was isolated using the RNeasy Minikit (QIAGEN #74106; Hilden, Germany) and precipitated by the ethanol/sodium acetate method. RNA concentration and quality was initially measured using a Nanodrop 2000 (ThemoFisher). Secondary analysis of concentration and quality was conducted by the Genomics CoRE Facility at the Icahn School of Medicine at Mount Sinai using Qubit RNA BR Assay Kit (ThermoFisher #Q10211). Library construction and RNA sequencing was performed by Novogene (Durham, NC).

*Tissue processing*

Four mice from each group (GR100, HBA, and GFP) were processed for sequencing, providing three distinct brain regions (Cortex (*CTX*), Frontal Cortex (*FC*), and Hippocampus (*HP*)) per mouse. After assessing sample quality, one Frontal Cortex sample was excluded due to poor quality, and all tissue samples from a single mouse were removed due to sample misclassification.

*Gene expression*

Reads were processed using the NGS-Data-Charmer pipeline. Briefly, adaptors and low-quality bases were trimmed from reads, which were then aligned to the mm10 genome using HISAT2 (version 2.2.1). Read counts in the mm10 GENCODE annotation (version M22) were generated using FeatureCounts DESeq2 (version 1.24.0, R version 3.6.1) was then used to calculate

differential expression from the read counts. The R package 'biomaRt' (version 2.40.5) was used to translate ensembl ids into common gene symbols.

*Gene ontology*

Mouse genes involved in inflammatory processes were extracted from the Mouse Genome Informatics group database (MGI). MGI mouse genes with the GO term 'Inflammatory response' were extracted. Ingenuity Pathway Analysis was applied to all differential genes identified in the previous analysis.

*Quantitative reverse transcription PCR*

For qPCR analysis, gene expression was measured in 4 replicates by PowerUP SYBR Green Master Mix (ThermoFisher # A25778) using an ABI PRISM 7900HT Sequence Detection System. Hypoxanthine phosphoribosyltransferase (*Hprt*) expression level was used as an internal control and data was normalized using the $2^{-\Delta\Delta Ct}$ method55. Levels of target gene mRNA was expressed relative to those of GFP + Veh mice for *in vivo* studies. Primers used in this study were designed using Primer-BLAST software (Ye et al., 2012) and are listed in Supplementary Table S1.

*Statistical Analysis*

All figure values are presented as mean and standard error of the mean (s.e.m.). Statistical tests are indicated in the figure legends. A confidence interval of 95% was used for all analyses. In all studies, outliers (> 2 SD from the mean) were excluded. All statistical analysis was performed using GraphPad Prism 9 software (GraphPad Software, San Diego CA). *$p < 0.05$, **$p < 0.01$, ***$p<0.001$, ****$p<0.0001$, ns not significant. Statistically insignificant trends are indicated by *p*-value.

## References


1. Cook, C. & Petrucelli, L. Genetic Convergence Brings Clarity to the Enigmatic Red Line in ALS. *Neuron* **101**, 1057–1069 (2019).
2. Renton, A. E. *et al.* A Hexanucleotide Repeat Expansion in C9ORF72 Is the Cause of Chromosome 9p21-Linked ALS-FTD. *Neuron* **72**, 257–268 (2011).
3. Mackenzie, I. R. *et al.* Dipeptide repeat protein pathology in C9ORF72 mutation cases: clinico-pathological correlations. *Acta Neuropathologica* **126**, 859–879 (2013).
4. Saberi, S. *et al.* Sense-encoded poly-GR dipeptide repeat proteins correlate to neurodegeneration and uniquely co-localize with TDP-43 in dendrites of repeat-expanded C9orf72 amyotrophic lateral sclerosis. **135**, 459–474 (2018).
5. Trageser, K. J., Smith, C., Herman, F. J., Ono, K. & Pasinetti, G. M. Mechanisms of Immune Activation by c9orf72-Expansions in Amyotrophic Lateral Sclerosis and Frontotemporal Dementia. *Frontiers in Neuroscience* **13**, (2019).
6. Zhang, Y. J. *et al.* Poly(GR) impairs protein translation and stress granule dynamics in C9orf72-associated frontotemporal dementia and amyotrophic lateral sclerosis. *Nature Medicine* **24**, 1136–1142 (2018).
7. Clarke, B. E. & Patani, R. The microglial component of amyotrophic lateral sclerosis. *Brain* **143**, 3526–3539 (2020).
8. Su, W. *et al.* Recombinant adeno-associated viral (rAAV) vectors mediate efficient gene transduction in cultured neonatal and adult microglia. *Journal of Neurochemistry* **136**, 49–62 (2016).
9. Corcia, P. *et al.* Molecular Imaging of Microglial Activation in Amyotrophic Lateral Sclerosis. *PLoS ONE* **7**, (2012).
10. Clarner, T. *et al.* CXCL10 Triggers Early Microglial Activation in the Cuprizone Model. *The Journal of Immunology* **194**, 3400–3413 (2015).
11. McGeough, M. D. *et al.* TNF regulates transcription of NLRP3 inflammasome components and inflammatory molecules in cryopyrinopathies. *Journal of Clinical Investigation* **127**, 4488–4497 (2017).
12. Zhang, X. *et al.* In vivo stress granule misprocessing evidenced in a FUS knock-in ALS mouse model. *Brain* **143**, 1350–1367 (2020).
13. Peters, O. M., Ghasemi, M. & Brown, R. H. Emerging mechanisms of molecular pathology in ALS. *Journal of Clinical Investigation* vol. 125 1767–1779 (2015).
14. Thonhoff, J. R., Simpson, E. P. & Appel, S. H. Neuroinflammatory mechanisms in amyotrophic lateral sclerosis pathogenesis. *Current opinion in neurology* vol. 31 635–639 (2018).
15. Heneka, M. T. *et al.* NLRP3 is activated in Alzheimer's disease and contributes to pathology in APP/PS1 mice. *Nature* **493**, 674–678 (2013).

16. Fan, Z. *et al.* Systemic activation of NLRP3 inflammasome and plasma α-synuclein levels are correlated with motor severity and progression in Parkinson's disease. *Journal of Neuroinflammation* **17**, 11 (2020).
17. Malhotra, S. *et al.* NLRP3 inflammasome as prognostic factor and therapeutic target in primary progressive multiple sclerosis patients. *Brain* **143**, 1414–1430 (2020).
18. Sanagi, T. *et al.* Appearance of phagocytic microglia adjacent to motoneurons in spinal cord tissue from a presymptomatic transgenic rat model of amyotrophic lateral sclerosis. *Journal of Neuroscience Research* **88**, 2736–2746 (2010).
19. Wang, R., Yang, B. & Zhang, D. Activation of interferon signaling pathways in spinal cord astrocytes from an ALS mouse model. *GLIA* **59**, 946–958 (2011).
20. Turner, M. R., Goldacre, R., Ramagopalan, S., Talbot, K. & Goldacre, M. J. Autoimmune disease preceding amyotrophic lateral sclerosis: an epidemiologic study. *Neurology* **81**, 1222–5 (2013).
21. Turner, M. R. *et al.* Evidence of widespread cerebral microglial activation in amyotrophic lateral sclerosis: An [11C](R)-PK11195 positron emission tomography study. *Neurobiology of Disease* **15**, 601–609 (2004).
22. Baron, R., Babcock, A. A., Nemirovsky, A., Finsen, B. & Monsonego, A. Accelerated microglial pathology is associated with Aβ plaques in mouse models of Alzheimer's disease. *Aging Cell* **13**, 584–595 (2014).
23. Debye, B. *et al.* Neurodegeneration and NLRP3 inflammasome expression in the anterior thalamus of SOD1(G93A) ALS mice. *Brain Pathology* **28**, 14–27 (2018).
24. Moreno-García, L. *et al.* Inflammasome in als skeletal muscle: Nlrp3 as a potential biomarker. *International Journal of Molecular Sciences* **22**, 1–15 (2021).
25. Johann, S. *et al.* NLRP3 inflammasome is expressed by astrocytes in the SOD1 mouse model of ALS and in human sporadic ALS patients. *GLIA* **63**, 2260–2273 (2015).
26. Provoost, S. *et al.* NLRP3/Caspase-1–Independent IL-1β Production Mediates Diesel Exhaust Particle-Induced Pulmonary Inflammation. *The Journal of Immunology* **187**, 3331–3337 (2011).
27. Klein, R. S. *et al.* Neuronal CXCL10 Directs CD8+ T-Cell Recruitment and Control of West Nile Virus Encephalitis. *Journal of Virology* **79**, 11457–11466 (2005).
28. Sasaki, S. Endoplasmic Reticulum Stress in Motor Neurons of the Spinal Cord in Sporadic Amyotrophic Lateral Sclerosis. *Journal of Neuropathology and Experimental Neurology* **69**, 346–355 (2010).
29. Perner, C. *et al.* Dysregulation of chemokine receptor expression and function in leukocytes from ALS patients. *Journal of Neuroinflammation* vol. 15 1–5 (2018).
30. Glascock, J. J. *et al.* Delivery of therapeutic agents through intracerebroventricular (ICV) and intravenous (IV) injection in mice. *Journal of visualized experiments: JoVE* (2011) doi:10.3791/2968.
31. Seibenhener, M. L. & Wooten, M. C. Use of the open field maze to measure locomotor and anxiety-like behavior in mice. *Journal of Visualized Experiments* (2015) doi:10.3791/52434.
32. Aartsma-Rus, A. & van Putten, M. Assessing functional performance in the Mdx mouse model. *Journal of Visualized Experiments* (2014) doi:10.3791/51303.

753 33. Paxinos and Franklin's the Mouse Brain in Stereotaxic Coordinates, Compact - 5th
754 Edition. https://www.elsevier.com/books/paxinos-and-franklins-the-mouse-brain-in-
755 stereotaxic-coordinates-compact/franklin/978-0-12-816159-3.
756 34. Saura, J., Tusell, J. M. & Serratosa, J. High-Yield Isolation of Murine Microglia by Mild
757 Trypsinization. *GLIA* **44**, 183–189 (2003).
758 35. Livak, K. J. & Schmittgen, T. D. Analysis of relative gene expression data using real-time
759 quantitative PCR and the 2-ΔΔCT method. *Methods* **25**, 402–408 (2001).
760 36. Ye, J. *et al.* Primer-BLAST: a tool to design target-specific primers for polymerase chain
761 reaction. *BMC bioinformatics* **13**, 134 (2012).
762